Nonlinear diffraction of light beams propagating in photorefractive media with embedded reflecting wire

E. G. Khamis,[1,*] A. Gammal,[1,†] G. A. El,[2,‡] Yu. G. Gladush,[3,§] and A. M. Kamchatnov[3,‖]
[1]*Instituto de Física, Universidade de São Paulo, 05315-970, C.P. 66318 São Paulo, Brazil*
[2]*Department of Mathematical Sciences, Loughborough University, Loughborough LE11 3TU, United Kingdom*
[3]*Institute of Spectroscopy, Russian Academy of Sciences, Troitsk, Moscow Region 142190, Russia*
(Received 4 February 2008; revised manuscript received 6 April 2008; published 21 July 2008)

The theory of nonlinear diffraction of intensive light beams propagating through photorefractive media is developed. Diffraction occurs on a reflecting wire embedded in the nonlinear medium at a relatively small angle with respect to the direction of the beam propagation. It is shown that this process is analogous to the generation of waves by a flow of a superfluid past an obstacle. The "equation of state" of such a superfluid is determined by the nonlinear properties of the medium. On the basis of this hydrodynamic analogy, the notion of the "Mach number" is introduced where the transverse component of the wave vector plays the role of the fluid velocity. It is found that the Mach cone separates two regions of the diffraction pattern: inside the Mach cone oblique dark solitons are generated and outside the Mach cone the region of "optical ship waves" (the wave pattern formed by a two-dimensional packet of linear waves) is situated. Analytical theory of the "optical ship waves" is developed and two-dimensional dark soliton solutions of the generalized two-dimensional nonlinear Schrödinger equation describing the light beam propagation are found. Stability of dark solitons with respect to their decay into vortices is studied and it is shown that they are stable for large enough values of the Mach number.

DOI: 10.1103/PhysRevA.78.013829 PACS number(s): 42.65.Tg, 42.65.Hw

I. INTRODUCTION

An analogy between propagation of light beams in nonlinear media and superfluid flow is well known and quite suggestive. Formally, it is based on a mathematical similarity of the equations for electromagnetic field evolution in light beams in paraxial approximation and the Gross-Pitaevskii equations for superfluid motion of Bose-Einstein condensates of dilute gases. Accordingly, such nonlinear structures as bright or dark solitons and vortices have been thoroughly studied both in optics and superfluid dynamics (see, e.g., [1,2]). These structures arise as results of interplay of nonlinear and dispersive properties of the medium under consideration. One more example of such a structure is provided by the so-called dispersive shocks which replace usual dissipative shocks of compressible fluid dynamics in the case when dissipation can be neglected compared with dispersive effects. As a result, a thin layer with strong dissipation within is replaced by an expanding region filled with fast nonlinear oscillations, which can be represented as a modulated nonlinear periodic wave (a "soliton lattice"). The notion of dispersive shocks arose first in water wave dynamics (the theory of undular bores on rivers) [3] and plasma physics (collisionless shock waves) [4], then the generality of this phenomenon was realized and (based on the Whitham theory [5] of modulations of nonlinear waves) mathematical methods for their description have been developed [6–12].

Realization of a Bose-Einstein condensate of dilute cold gases [13–15] and study of its dynamics has naturally led to the theoretical and experimental studies of dispersive shocks in this new medium [16–20]. The corresponding optical counterpart of dispersive shocks suggested by the above mentioned analogy between beam optics and superfluid dynamics was realized experimentally in [21–24] and the theory of such optical dispersive shocks was developed in [25].

In dissipative fluid dynamics with negligible dispersion the shocks can also be generated by a supersonic flow of the fluid past an obstacle. Such shocks have the form of a sharp stationary jump of the fluid parameters across certain lines inclined with respect to the flow direction. For shocks of small intensity these lines lie along the so-called "Mach cones" (see, e.g., [26]). In dispersive fluid dynamics these oblique shocks unfold into "fans" of spatial solitons spreading downstream from the obstacle [27]. The theory of such oblique dispersive shocks was developed in [28] for the case of weakly dispersive media when the flow past a slender body is asymptotically described by the Korteweg–de Vries equation along the Mach lines.

Dynamics of a Bose-Einstein condensate is described by the Gross-Pitaevskii equation and the theory of oblique dispersive shocks was extended to this case in [29]. If the obstacle is small enough, then the dispersive shock degenerates into a single oblique dark soliton. The theory of oblique dark solitons was developed in [30,31]. It is important to note that such oblique solitons are located inside the Mach cone with the Mach number defined as a ratio of the flow velocity to the sound speed calculated at infinite wavelength. The linear wave pattern formed by a stationary two-dimensional modulated wave packet of Bogoliubov excitations and having the same nature as the classical fluid dynamics Kelvin "ship-

*egkhamis@if.usp.br
†gammal@if.usp.br
‡G.El@lboro.ac.uk
§gladush@isan.troitsk.ru
‖kamch@isan.troitsk.ru

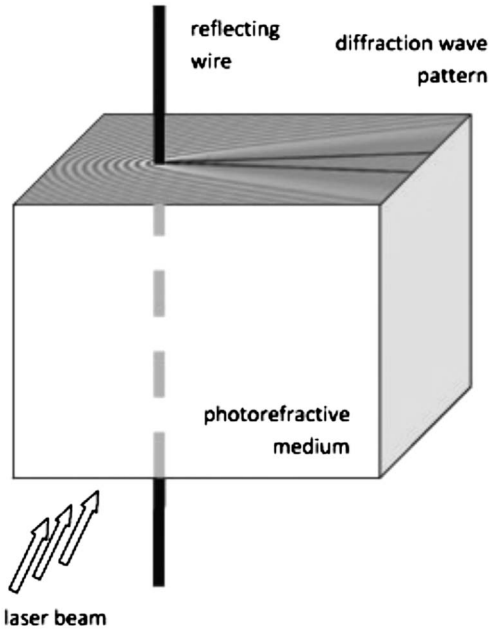

FIG. 1. A sketch of formation of nonlinear diffraction pattern in propagation of a light beam through photorefractive medium with embedded reflecting wire.

wave" phenomenon (see, e.g., [32]) is located outside the Mach cone. Apparently, these Bogoliubov "ship waves" were observed in the experiment [33] and their theory was developed in [34,35]. The analogy between beam optics and superfluid dynamics suggests that similar effects would exist in the optical context where they take the form of diffraction wave patterns in light beams propagating through a nonlinear medium. Although such structures were observed in some experiments (see, e.g., [36]), they have not been studied systematically yet. In this paper, we shall consider a typical simple situation of nonlinear diffraction of light which can be considered as an optical counterpart of generation of spatial dispersive shocks and ship waves in the flow of Bose-Einstein condensate past an obstacle. To be definite, we consider a light beam propagating through a bulk self-defocusing nonlinear refractive medium with a thin wire (a "needle") inserted in it; see Fig. 1. Direction of the light beam is tilted with respect to the wire; that is, there exists a "flow of light past an obstacle." As a result, at the output plane of the medium a diffraction pattern is formed consisting of oblique dark solitons and ship waves. We shall give here analytical and numerical treatment of this phenomenon and obtain main characteristics of the diffraction pattern.

II. MAIN EQUATIONS AND GENERAL FORM OF THE DIFFRACTION PATTERN

Propagation of stationary light beams is described by the equation

$$i\frac{\partial\psi}{\partial z}+\frac{1}{2k_0}\Delta_\perp\psi+\frac{k_0}{n_0}\delta n(|\psi|^2)\psi+V(\mathbf{r})\psi=0, \tag{1}$$

where ψ is the envelope field strength of the electromagnetic wave with the wave number $k_0=2\pi n_0/\lambda$, z is the coordinate along the beam, x,y are transverse coordinates, $\mathbf{r}=(x,y)$, $\Delta_\perp=\partial^2/\partial x^2+\partial^2/\partial y^2$ is the transverse Laplacian, n_0 is the linear refractive index, $V(\mathbf{r})$ represents a "potential" of an obstacle (e.g., a reflecting wire) at which diffraction occurs, and in a photorefractive medium we have

$$\delta n=-\frac{1}{2}n_0^3r_{33}E_p\frac{\rho}{\rho+\rho_d}, \tag{2}$$

where E_p is the electric field applied to the crystal, r_{33} is the electro-optical index, $\rho=|\psi|^2$, and ρ_d is the saturation parameter.

For mathematical convenience, we introduce nondimensional variables

$$\tilde{z}=\frac{1}{2}k_0n_0^2r_{33}E_p\left(\frac{\rho_c}{\rho_d}\right)z,\quad \tilde{x}=k_0n_0\sqrt{\frac{1}{2}r_{33}E_p\left(\frac{\rho_c}{\rho_d}\right)}x,$$

$$\tilde{y}=k_0n_0\sqrt{\frac{1}{2}r_{33}E_p\left(\frac{\rho_c}{\rho_d}\right)}y,\quad \tilde{\psi}=\sqrt{\rho_c}\psi, \tag{3}$$

where ρ_c is a characteristic value of optical intensity (its concrete definition depends on the problem under consideration; for instance, it can be the background intensity), so that Eq. (1) takes the form of the generalized nonlinear Schrödinger (GNLS) equation

$$i\frac{\partial\psi}{\partial z}+\frac{1}{2}\Delta_\perp\psi-\frac{|\psi|^2}{1+\gamma|\psi|^2}\psi+V(\mathbf{r})\psi=0, \tag{4}$$

where $\gamma=\rho_c/\rho_d$, $V(\mathbf{r})$ is represented in nondimensional units, and tildes are omitted for convenience of the notation. In fact, our approach can be applied to other forms of the nonlinear term provided it corresponds to self-defocusing light beams. Therefore we shall also use the general form of the equation,

$$i\frac{\partial\psi}{\partial z}+\frac{1}{2}\Delta_\perp\psi-f(|\psi|^2)\psi+V(\mathbf{r})\psi=0, \tag{5}$$

where $f(|\psi|^2)>0$, In particular, for the photorefractive medium,

$$f(\rho)=\rho/(1+\gamma\rho). \tag{6}$$

If the saturation effect is negligibly small ($\gamma|\psi|^2\ll1$), then Eq. (4) reduces to the standard cubic nonlinear Schrödinger (NLS) equation

$$i\frac{\partial\psi}{\partial z}+\frac{1}{2}\Delta_\perp\psi-|\psi|^2\psi+V(\mathbf{r})\psi=0. \tag{7}$$

If the phase of ψ is a single-valued function, then it is convenient to represent the above NLS equations in a fluid dynamics type form by means of the substitution

$$\psi(\mathbf{r},z)=\sqrt{\rho}\exp\left[i\int^{\mathbf{r}}\mathbf{u}(\mathbf{r}',z)\cdot d\mathbf{r}'\right], \tag{8}$$

so that they are transformed into

$$\rho_z+\nabla_\perp\cdot(\rho\mathbf{u})=0,$$

$$\mathbf{u}_z + (\mathbf{u}\cdot\boldsymbol{\nabla}_\perp)\mathbf{u} + \boldsymbol{\nabla}_\perp f(\rho) - \boldsymbol{\nabla}V(\mathbf{r}) - \boldsymbol{\nabla}_\perp\left(\frac{\Delta_\perp\rho}{4\rho} - \frac{(\boldsymbol{\nabla}_\perp\rho)^2}{8\rho^2}\right) = 0. \tag{9}$$

In the hydrodynamic interpretation the light intensity ρ has a meaning of a density of a "fluid" and Eq. (6) can be viewed as an "equation of state" for such a fluid. The function $\mathbf{u}(\mathbf{r},z)$ is a local value of the wave vector component transverse to the direction of the light beam; in hydrodynamic representation it has a meaning of the "flow velocity." The variable z plays the role of time so it is natural to describe the deformations of the light beam in evolutionary terms. We note that substitution (8) rules out vorticity so that system (9) actually represents a restriction of the multidimensional GNLS Eq. (5) to potential "flows."

We shall consider propagation of a tilted light beam with uniform input intensity, that is, at $z=0$ it has the initial form

$$\psi(\mathbf{r},0) = \exp(iUx), \tag{10}$$

that is, we suppose that the background intensity is equal to unity; U represents the x component of the wave vector due to tilting of the light beam. The problem is to describe the wave pattern at the output value of z.

To clarify a general picture of the diffraction pattern (see Fig. 2), we have solved Eq. (4) numerically for the initial wave function ψ given by Eq. (10) with $U=2$ and the boundary condition of vanishing ψ at the surface $r=1$ of the obstacle located at $x=0$, $y=0$. As we see, the diffraction pattern consists of two different parts separated by the Mach (or Cherenkov) cone which is defined by the lines drawn at angle θ with respect to the direction of the flow (x axis) with

$$\sin\theta = \frac{1}{M}, \quad M = \frac{U}{c_s}, \tag{11}$$

where the sound velocity corresponds to the dispersionless limit of Eqs. (9), that is $[\boldsymbol{\nabla}p/\rho \equiv \boldsymbol{\nabla}f(\rho)]$

$$c_s = \sqrt{\left.\frac{dp}{d\rho}\right|_{\rho_0}} = \sqrt{f'(\rho_0)\rho_0} \tag{12}$$

which in the photorefractive case with $\rho_0=1$ yields

$$c_s = \frac{1}{1+\gamma} \quad \text{and} \quad M = U(1+\gamma). \tag{13}$$

Outside the Mach cone there is a stationary wave pattern created by interference of linear (far enough from the obstacle) waves. Inside the Mach cone there are two oblique dark solitons situated symmetrically with respect to the direction of the flow. These oblique solitons decay at the end points into vortices but closer to the obstacle they are described by a potential flow with the jump of phase across them as is demonstrated in Fig. 3.

Our task now is to develop analytical theory for these two regions of the diffraction pattern and to compare it with numerical simulations. We shall start with the ship-waves pattern located outside the Mach cone.

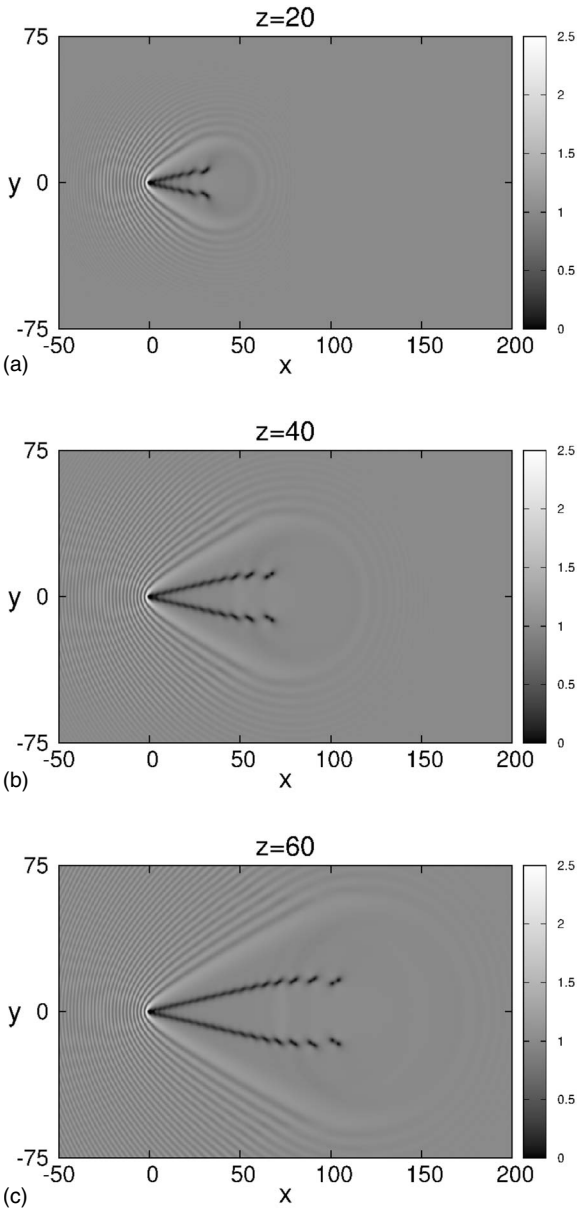

FIG. 2. Evolution of the diffraction pattern at the output plane as a function of the length z of the photorefractive medium. The patterns are obtained by numerical solution of Eq. (4) with $V(\mathbf{r})$ corresponding to an ideally reflecting wire with unit radius for $\gamma=0.2$, $U=2$, and (a) $z=20$, (b) $z=40$, (c) $z=60$. Results of numerical simulations here and below are presented in nondimensional units defined in Eq. (3).

III. DIFFRACTION PATTERN OUTSIDE THE MACH CONE

If the size of the obstacle is much less than the wavelength of the pattern, then we can consider it as a pointlike one and take the obstacle potential in the form

$$V(\mathbf{r}) = V_0\delta(\mathbf{r}). \tag{14}$$

Far enough from the obstacle, the amplitude of the wave pattern is small compared with the background intensity of

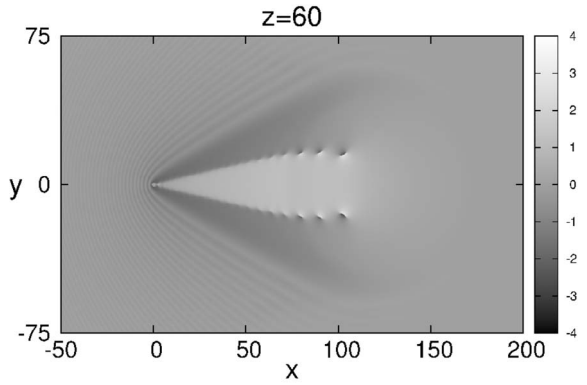

FIG. 3. Distribution of the phase in the diffraction pattern at the output plane of the photorefractive medium. The pattern corresponds to $\gamma=0.2$, $U=2$, and $z=60$.

the light beam. Hence the wave pattern can be calculated by means of perturbation theory [37].

If we neglect the influence of the obstacle, then the ψ function of a uniform light beam with the intensity ρ_0 depends on z in the reference frame with $U=0$ as $\psi \propto \exp[-if(\rho_0)z]$. We eliminate this dependence by introducing the substitution $\psi=\Psi\cdot\exp[-if(\rho_0)z]$ so that Ψ satisfies the equation

$$i\Psi_z + \frac{1}{2}\Delta\psi + [f(\rho_0) - f(|\Psi|^2)]\Psi = 0. \tag{15}$$

In the same reference frame the obstacle moves with the velocity $-\mathbf{U}$ and generates diffraction waves which in the linear approximation are described by a small correction $\delta\Psi$ to the unperturbed wave function: $\Psi \approx \sqrt{\rho_0} + \delta\Psi$. Hence $\delta\Psi$ satisfies the equation

$$i\delta\Psi_z + \frac{1}{2}\Delta\delta\Psi - c_s^2(\delta\Psi + \delta\Psi^*) - V_0\sqrt{\rho_0}\delta(\mathbf{r} + \mathbf{U}z) = 0, \tag{16}$$

where we have added the potential of the obstacle due to which linear waves are generated. In the stationary case, which we are interested in, the wave pattern moves with the obstacle, that is, in the reference frame attached to the reflecting wire we have $\Psi=\Psi(\mathbf{r}+\mathbf{U}z)$ and

$$\frac{\partial}{\partial z}\delta\Psi(\mathbf{r} + \mathbf{U}z) = (\mathbf{U}\cdot\nabla)\delta\Psi(\mathbf{r} + \mathbf{U}z).$$

Introducing $\mathbf{r}'=\mathbf{r}+\mathbf{U}z$ and omitting primes, we arrive at the equation

$$i(\mathbf{U}\cdot\nabla)\delta\Psi + \frac{1}{2}\Delta\delta\Psi - c_s^2(\delta\Psi + \delta\Psi^*) - V_0\sqrt{\rho_0}\delta(\mathbf{r}) = 0, \tag{17}$$

describing stationary diffraction pattern generated by the beam.

Equation (17) can be solved by the Fourier method. We introduce the Fourier transform of the wave function:

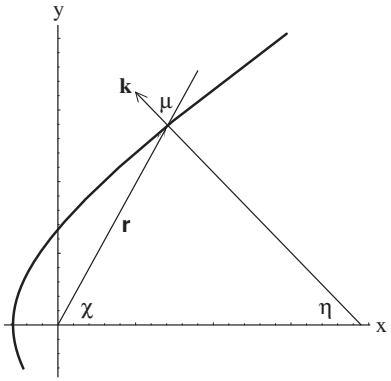

FIG. 4. Coordinates defining a radius vector $\mathbf{r}$ and a wave vector $\mathbf{k}$, normal to the wave front shown schematically by a curved line.

$$\delta\Psi = \int \delta\Psi_{\mathbf{k}} e^{i\mathbf{k}\cdot\mathbf{r}}\frac{d^2k}{(2\pi)^2}, \quad \delta\Psi^* = \int \delta\Psi^*_{\mathbf{k}} e^{-i\mathbf{k}\cdot\mathbf{r}}\frac{d^2k}{(2\pi)^2} \tag{18}$$

and obtain

$$-(\mathbf{k}\cdot\mathbf{U} + k^2/2 + c_s^2)\delta\Psi_{\mathbf{k}} - c_s^2\delta\Psi^*_{-\mathbf{k}} = V_0\sqrt{\rho_0}. \tag{19}$$

Another equation is obtained by means of substitution $\mathbf{k}\rightarrow-\mathbf{k}$ and complex conjugation:

$$-c_s^2\delta\Psi_{\mathbf{k}} + (\mathbf{k}\cdot\mathbf{U} - k^2/2 - c_s^2)\delta\Psi^*_{-\mathbf{k}} = V_0\sqrt{\rho_0}. \tag{20}$$

Solution of Eqs. (19) and (20) reads

$$\delta\Psi_{\mathbf{k}} = V_0\sqrt{\rho_0}\frac{k^2/2 - \mathbf{k}\cdot\mathbf{U}}{(\mathbf{k}\cdot\mathbf{U})^2 - k^2(c_s^2 + k^2/4)}. \tag{21}$$

Since

$$\delta\rho = \sqrt{\rho_0}(\delta\Psi + \delta\Psi^*) = \int (\delta\Psi_{\mathbf{k}} + \delta\Psi^*_{-\mathbf{k}})e^{i\mathbf{k}\cdot\mathbf{r}}\frac{d^2k}{(2\pi)^2}$$

we arrive at the following expression for the intensity perturbation in the output diffraction wave pattern created by propagation of light past a reflecting wire:

$$\delta\rho = V_0\rho_0\int \frac{k^2 e^{i\mathbf{k}\cdot\mathbf{r}}}{(\mathbf{k}\cdot\mathbf{U})^2 - k^2(c_s^2 + k^2/4) + i0}\frac{d^2k}{(2\pi)^2}, \tag{22}$$

where we have introduced an infinitesimal positive imaginary term $+i0$ corresponding to the radiation condition for outgoing waves.

Now we introduce polar coordinates (see Fig. 4) defining the components of the vectors $\mathbf{r}$ and $\mathbf{k}$ as

$$x = r\cos\chi, \quad y = r\sin\chi;$$

$$k_x = -k\cos\eta, \quad k_y = k\sin\eta. \tag{23}$$

Simple transformation casts Eq. (22) in the form

$$\delta\rho = \frac{V_0\rho_0}{\pi^2}\int_{-\pi}^{\pi}\int_0^{\infty}\frac{ke^{-ikr\cos(\chi+\eta)}dkd\eta}{k^2 - k_0^2 - i0}, \tag{24}$$

where

$$k_0 = 2c_s\sqrt{M^2\cos^2\eta - 1} = c_s\tilde{k}(\eta). \tag{25}$$

We can represent the integral (24) as a sum

$$\int_{-\pi/2}^{3\pi/2} d\eta = \int_{-\pi/2}^{\pi/2} d\eta + \int_{\pi/2}^{3\pi/2} d\eta$$

and, noticing that the second term after substitution $\eta' = \eta - \pi$ becomes equal to a complex conjugate of the first one, we rewrite it as

$$\delta\rho = \frac{V_0\rho_0}{\pi^2}\mathrm{Re}\int_{-\pi/2}^{\pi/2}\int_0^\infty \frac{ke^{-ikr\cos(\chi+\eta)}dkd\eta}{k^2 - k_0^2 - i0}. \tag{26}$$

To perform integration over k, we notice that the integrand function has a pole in the first quadrant,

$$k = \sqrt{k_0^2 + i0} = k_0 + i0, \tag{27}$$

which gives the main contribution into the integral for $\cos(\chi+\eta) < 0$. Indeed, taking a closed contour along the positive real axis of k with added quarter of the circle, which gives no contribution into the integral, and a path along positive imaginary axis which contribution

$$\int_0^\infty \frac{ke^{-kr\cos(\chi+\eta)}dk}{k^2 + k_0^2} \propto \frac{1}{r^2} \tag{28}$$

is decreasing with r much faster than the contribution of the pole (which is proportional to $r^{-1/2}$; see below), we obtain

$$\delta\rho = -\frac{2V_0\rho_0}{\pi}\,\mathrm{Im}\int_{-\pi/2}^{\pi/2} e^{-ikr\cos(\chi+\eta)}d\eta, \tag{29}$$

where k is determined by Eq. (25) (index "0" is omitted here).

If the phase $\mathbf{k}\cdot\mathbf{r} = r\varphi$, where

$$\varphi(\eta) = k(\eta)\cos(\chi + \eta) \tag{30}$$

is large enough, the integral (29) can be evaluated by the standard method of stationary phase. This condition is fulfilled far enough from the obstacle $r \to \infty$ provided $|k(\eta)\cos(\chi+\eta)| \gg 1/r$. The equation which determines the point of the stationary phase $\partial\varphi/\partial\eta = 0$ gives relationships for the angles (see Fig. 4)

$$\tan\mu = \frac{2U^2}{k^2}\sin 2\eta = \frac{2M^2}{\tilde{k}^2}\sin 2\eta,$$

$$\tan\chi = \frac{(c_s^2 + k^2/2)\tan\eta}{U^2 - (c_s^2 + k^2/2)} = \frac{(1 + \tilde{k}^2/2)\tan\eta}{M^2 - (1 + \tilde{k}^2/2)}. \tag{31}$$

Taking into account Eq. (25), we find

$$\cos\mu = \frac{\tilde{k}^2}{2[(M^2-2)\tilde{k}^2 + 4(M^2-1)]^{1/2}}. \tag{32}$$

With account of Eq. (31), we get the expression for the second derivative of the phase,

$$\frac{\partial^2\varphi}{\partial\eta^2} = 8\frac{\cos\mu}{\tilde{k}^3}[(M^2-2)\tilde{k}^2 + 6(M^2-1)]. \tag{33}$$

As a result, the expression for the condensate density (29) assumes the form

$$\delta\rho = V_0\rho_0\sqrt{\frac{2\tilde{k}}{\pi r}}\frac{[(M^2-2)\tilde{k}^2 + 4(M^2-1)]^{1/4}}{[(M^2-2)\tilde{k}^2 + 6(M^2-1)]^{1/2}} \times\cos\left(c_s\tilde{k}r\cos\mu - \frac{\pi}{4}\right), \tag{34}$$

where

$$\tilde{k} = 2\sqrt{M^2\cos^2\eta - 1}. \tag{35}$$

As we see from Eq. (34), the linear waves exist only in the region

$$-\arccos(1/M) \le \eta \le \arccos(1/M) \tag{36}$$

outside the Mach cone.

With the help of Eqs. (31) one can find the shape of the lines of constant phase (e.g., wave crests) $\Phi = kr\cos\mu$ in a parametric form,

$$x = r\cos\chi = \frac{4\Phi}{c_s\tilde{k}^3}\cos\eta(1 - M^2\cos 2\eta),$$

$$y = r\sin\chi = \frac{4\Phi}{c_s\tilde{k}^3}\sin\eta(2M^2\cos^2\eta - 1). \tag{37}$$

Small values of η correspond to waves in front of the obstacle. In this case we have

$$x \cong -\frac{\Phi}{2c_s\sqrt{M^2-1}} + \frac{(2M^2-1)\Phi}{4c_s(M^2-1)^{3/2}}\eta^2,$$

$$y \cong \frac{(2M^2-1)\Phi}{2c_s(M^2-1)^{3/2}}\eta, \tag{38}$$

that is, the lines of stationary phase take parabolic form

$$x(y) \cong -\frac{\Phi}{2c_s\sqrt{M^2-1}} + \frac{c_s(M^2-1)^{3/2}}{(2M^2-1)\Phi}y^2. \tag{39}$$

The limiting values $\eta = \pm\arccos(1/M)$ correspond to the lines

$$\frac{x}{y} = \pm\sqrt{M^2-1}, \tag{40}$$

i.e., far from the obstacle the lines approach to the straight lines parallel to those forming the Mach cone (11). Predictions of the analytical theory are compared with the numerically calculated wave pattern in Fig. 5 and excellent agreement is found.

In the region in front of the obstacle where $y = 0, x < 0$, the perturbations of the light intensity take the simplest form. Here we have

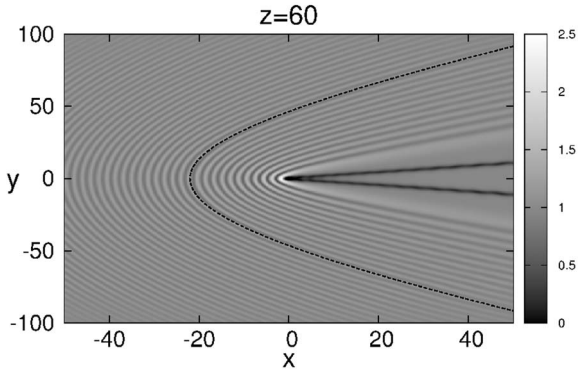

FIG. 5. Numerically calculated wave pattern corresponding to diffraction of a light beam on the obstacle embedded into a photorefractive medium. The plot corresponds to $\gamma=0.2$, $U=2$, and the radius of the reflecting wire to $r=1$. Dashed line corresponds to linear analytical theory, Eq. (37), for the line of constant phase; it is shifted to the left to two units of length from the center of the obstacle due to its finite size in numerical simulations and better fitting to numerics.

$$k = 2c_s\sqrt{M^2-1}, \tag{41}$$

i.e., the wavelength $\lambda=2\pi/k$ is constant and

$$\delta\rho = 2V_0\rho_0\sqrt{\frac{(M^2-1)^{1/2}}{\pi(2M^2+1)|x|}}\cos\left(-2c_s\sqrt{M^2-1}x-\frac{\pi}{4}\right),$$

$$y=0, \quad x<0. \tag{42}$$

The plot illustrating this dependence is shown in Fig. 6. As we see, approximate formula Eq. (34) is accurate enough almost everywhere except the small vicinity of the obstacle.

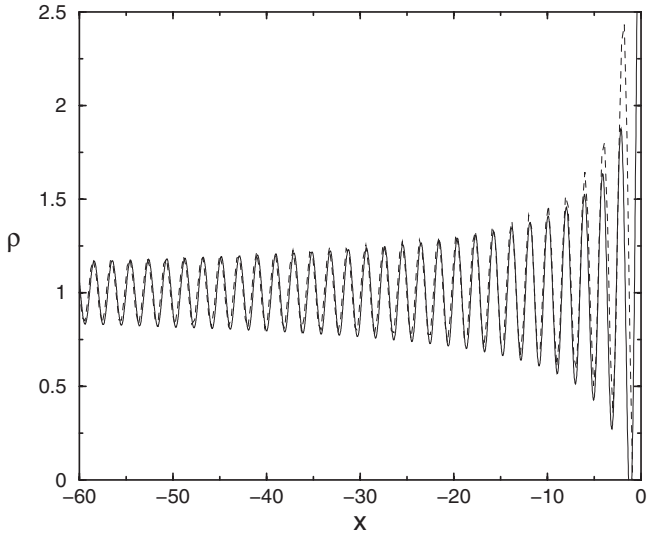

FIG. 6. Profile of intensity in front of the obstacle for $x<0$, $y=0$, and choice of the parameters $\gamma=0.2$, $U=2$, $V_0=2.6$. Solid line corresponds to Eq. (42) and dashed line to numerical solution of Eqs. (5) and (6).

As was indicated above, the method of stationary phase used for the derivation of Eq. (34) requires the condition $|k(\eta)\cos(\chi+\eta)| \gg 1/r$. According to Eq. (25) we have $k\to 0$ at the Mach cone and the necessary condition is not fulfilled. To find a wave pattern near the Mach cone one should return to the investigation of the integral (22) and introduce new coordinates along the Mach cone (ξ) and normal to it (τ) (i.e., they are rotated to the angle θ around the origin):

$$x = \xi\cos\theta - \tau\sin\theta, \quad y = \xi\sin\theta + \tau\cos\theta. \tag{43}$$

In new coordinates Eq. (22) takes the form

$$\delta\rho = V_0\rho_0\int\int \frac{k^2 e^{i(k_\xi\xi+k_\tau\tau)}}{(k_\xi U\cos\theta - k_\tau U\sin\theta)^2 - k^2(c_s^2+k^2/4)+i0} \times\frac{dk_\xi dk_\tau}{(2\pi)^2}. \tag{44}$$

Far from the obstacle, near the Mach cone, the dependence of the wave pattern on the ξ coordinate is much slower than the dependence on the τ coordinate; besides that, one has $|k|\ll 1$ here. The main contribution into the integral over k_ξ is due to the pole whose position is determined by the equations

$$(k_\xi U\cos\theta - k_\tau U\sin\theta)^2 - k^2(c_s^2+k^2/4)=0, \quad k_\xi^2+k_\tau^2=k^2. \tag{45}$$

Their approximate solution for $k_\xi \ll k_\tau \ll 1$ is given by

$$k_\xi = -\frac{k_\tau^3(1+\gamma)^2}{8\sqrt{M^2-1}}, \tag{46}$$

where we have taken into account Eq. (13). Integration over k_ξ yields

$$\delta\rho = \frac{V_0\rho_0(1+\gamma)^2}{2\sqrt{M^2-1}}\frac{\partial}{\partial\tau}\left[\frac{1}{\pi}\int_0^\infty \cos\left(\frac{k_\tau^3\xi(1+\gamma)^2}{8\sqrt{M^2-1}}-k_\tau\tau\right)dk_\tau\right], \tag{47}$$

and with account of the integral representation of the Airy function

$$\mathrm{Ai}(z) = \frac{1}{\pi}\int_0^\infty \cos\left(\frac{1}{3}\kappa^3+z\kappa\right)d\kappa \tag{48}$$

we obtain the following expression for the density oscillations in the vicinity of the Mach cone:

$$\delta\rho = -\frac{2V_0\rho_0}{(M^2-1)^{1/6}}\left(\frac{1+\gamma}{3\xi}\right)^{2/3}\mathrm{Ai}'\left(-\frac{2(M^2-1)^{1/6}}{[3(1+\gamma)^2\xi]^{1/3}}\tau\right), \tag{49}$$

where Ai′ denotes the first derivative of the Airy function with respect to its argument. Returning to x and y coordinates, we get

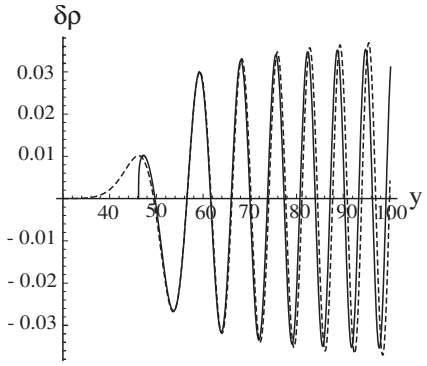

FIG. 7. Wave pattern near the Mach cone. Solid line corresponds to Eq. (34) and dashed line to Eq. (50).

$$\delta\rho = -\frac{2V_0\rho_0}{(M^2-1)^{1/6}}\left(\frac{1+\gamma}{3(x\cos\theta + y\sin\theta)}\right)^{2/3} \times \mathrm{Ai}'\left(-\frac{2(M^2-1)^{1/6}(-x\sin\theta + y\cos\theta)}{[3(1+\gamma)^2(x\cos\theta + y\sin\theta)]^{1/3}}\right), \quad (50)$$

where $\sin\theta = 1/M$, $\cos\theta = \sqrt{M^2-1}/M$.

The above formulas enable one to derive expressions for the dependence of intensity on the y coordinate for fixed value of x which may be convenient for comparison with the experiment and numerical simulations. Far enough from the Mach cone when Eq. (34) can be applied we find dependence of χ on y from the equation

$$\frac{y}{x} = \tan\chi = \frac{(1+\tilde{k}^2/2)\tan\eta}{M^2 - (1+\tilde{k}^2/2)}, \quad (51)$$

then

$$r(\eta) = \frac{y}{\sin\chi(\eta)}, \quad (52)$$

where $\tilde{k}(\eta)$ and $\mu(\eta)$ are defined by Eqs. (35) and (32). In the limit $y \gg x$ we have $\chi \to \pi/2$, hence the denominator in the right-hand side of Eq. (51) vanishes and

$$\tilde{k} \cong \sqrt{2(M^2-1)} \quad \text{for} \quad y \gg x. \quad (53)$$

Comparison with Eq. (35) gives the limiting value of η,

$$\cos\eta \cong \frac{\sqrt{M^2+1}}{\sqrt{2}M}. \quad (54)$$

Substitution of these values of the parameters into Eq. (34) yields

$$\delta\rho(y) \cong -V_0\rho_0\sqrt{\frac{2M}{\pi(M^2-1)y}} \times \cos[(M-1/M)y - \pi/4] \quad \text{for} \quad y \gg x. \quad (55)$$

The profile of the wave in the vicinity of the Mach cone is shown in Fig. 7. As we see, Eq. (34) reproduces the density profile very well almost everywhere except for a closest vicinity of the Mach cone and inside it where the density perturbation decays exponentially according to the behavior of the Airy function in Eq. (50).

IV. OBLIQUE DARK SOLITON

Far enough from the obstacle where vorticity is equal to zero and the light "flow" can be considered as potential, we can use the hydrodynamic representation of equations of light beam evolution. Here the potential of the obstacle can be neglected (in the case of a reflecting wire it obviously vanishes outside the surface of the wire, that is, the obstacle is represented by an infinite cylindrical barrier) and for large enough z the soliton is close to its stationary state. The profiles of intensity ρ and "velocities" u,v can be found analytically as a solution of stationary equations

$$(\rho u)_x + (\rho v)_y = 0, \quad (56)$$

and

$$uu_x + vu_y + \left(\frac{\rho}{1+\gamma\rho}\right)_x + \left(\frac{\rho_x^2+\rho_y^2}{8\rho^2} - \frac{\rho_{xx}+\rho_{yy}}{4\rho}\right)_x = 0,$$

$$uv_x + vv_y + \left(\frac{\rho}{1+\gamma\rho}\right)_y + \left(\frac{\rho_x^2+\rho_y^2}{8\rho^2} - \frac{\rho_{xx}+\rho_{yy}}{4\rho}\right)_y = 0, \quad (57)$$

with boundary conditions (in this section we assume $\rho_0 = 1$)

$$\rho = 1, \quad u = U, \quad v = 0 \quad \text{at} \quad |x| \to \infty. \quad (58)$$

To simplify calculations, it is convenient to notice that one of Eqs. (57) can be replaced by the condition of zero vorticity

$$u_y - v_x = 0 \quad (59)$$

which is fulfilled for the potential flow in the soliton solution.

We look for the solution in the form

$$\rho = \rho(\theta), \quad u = u(\theta), \quad v = v(\theta), \quad \text{where} \quad \theta = x - ay. \quad (60)$$

The parameter a determines a slope of the oblique soliton in the x,y plane. Then Eqs. (56) and (59) with account of conditions (58) give after simple calculation the expressions for the components of the "flow velocity" in terms of the light intensity

$$u = \frac{U(1+a^2\rho)}{(1+a^2)\rho}, \quad v = -\frac{aU(1-\rho)}{(1+a^2)\rho}. \quad (61)$$

Substitution of these expressions into any Eq. (57) and integration of the resulting equation yields

$$\frac{1}{8}(1+a^2)^2(\rho'^2 - 2\rho\rho'') + (1+a^2)\frac{\rho^3}{1+\gamma\rho} - \left(\frac{U^2}{2} + \frac{1+a^2}{1+\gamma}\right)\rho^2 + \frac{U^2}{2} = 0, \quad (62)$$

where an integration constant is chosen in accordance with the conditions (58). This equation can be integrated once more to give

$$\frac{(1+a^2)^2}{8}\left(\frac{d\rho}{d\theta}\right)^2 = -\frac{(1+a^2)\rho}{\gamma^2}\ln(1+\gamma\rho) + \left(\frac{1+a^2}{(1+\gamma)\gamma} - \frac{U^2}{2}\right)\rho^2 + \left(U^2 + \frac{1+a^2}{\gamma^2}\ln(1+\gamma) - \frac{1+a^2}{\gamma(1+\gamma)}\right)\rho - \frac{U^2}{2}, \tag{63}$$

where Eq. (58) is also taken into account. For a given Mach number $M=(1+\gamma)U$ the soliton solution depends on the slope parameter a alone.

Now we notice that expressions for the flow velocity field (61) in terms of intensity ρ do not depend on the nonlinear properties of the medium but are determined completely by the "continuity" equation and the condition (59) of potentiality of the flow. Therefore we can change the "reference frame" in such a way that the transversal velocity (wave vector **u**) is equal to zero at $|\theta|\to\infty$. This means that we rotate the reference frame to the angle $\phi=\arctan a$ and pass to the frame "moving" with "velocity" $(U\cos\phi, U\sin\phi)$ as z increases, which means the change of coordinates

$$\tilde{x} = x\cos\phi - y\sin\phi - U\cos\phi\cdot z,$$

$$\tilde{y} = x\sin\phi + y\cos\phi - U\sin\phi\cdot z. \tag{64}$$

Correspondingly, the velocity field transforms as

$$\tilde{u} = (u-U)\cos\phi - v\sin\phi,$$

$$\tilde{v} = (u-U)\sin\phi + v\cos\phi. \tag{65}$$

Substitution of Eq. (61) gives

$$\tilde{u} = c\left(\frac{1}{\rho} - 1\right), \quad \tilde{v} = 0, \tag{66}$$

where we have introduced the parameter

$$c = \frac{U}{\sqrt{1+a^2}}. \tag{67}$$

In new variables the velocity field does not have a component along the $\tilde{y}$ coordinate. The variable θ takes the form $\theta=\sqrt{1+a^2}(\tilde{x}+cz)$ and hence the intensity ρ does not depend on the $\tilde{y}$ coordinate. Thus in the new coordinate system we have a one-dimensional (1D) dark soliton moving with velocity c in the negative direction of the $\tilde{x}$ axis. This transformation will be used below in the study of stability of dark solitons.

The introduction of the parameter c permits one to represent Eq. (63) as

$$\frac{1}{8}\left(\frac{d\rho}{d\xi}\right)^2 = -\frac{\rho}{\gamma^2}\ln(1+\gamma\rho) + \left(\frac{1}{(1+\gamma)\gamma} - \frac{c^2}{2}\right)\rho^2 + \left(c^2 + \frac{1}{\gamma^2}\ln(1+\gamma) - \frac{1}{\gamma(1+\gamma)}\right)\rho - \frac{c^2}{2} \equiv Q(\rho), \tag{68}$$

where $\xi=\tilde{x}+cz$. The function $Q(\rho)$ has a double zero at $\rho=1$ which corresponds to the tails of soliton. Another zero at $\rho=\rho_m$ corresponds to the minimal intensity at the center of soliton, which is therefore related to the parameter c as

$$c = \frac{1}{1-\rho_m}\left[\frac{2\rho_m}{\gamma}\left(\frac{1}{\gamma}\ln\frac{1+\gamma}{1+\gamma\rho_m} - \frac{1-\rho_m}{1+\gamma}\right)\right]^{1/2}. \tag{69}$$

Taking into account Eq. (67) we find the expression for the slope a as a function of ρ_m:

$$a = \left(\frac{U^2(1-\rho_m)^2\gamma}{2\rho_m\{(1/\gamma)\ln[(1+\gamma)/(1+\gamma\rho_m)] - [(1-\rho_m)/(1+\gamma)]\}} - 1\right)^{1/2}. \tag{70}$$

The slope of the most shallow solitons with $\rho_m\to 1$ is equal to

$$a_{\min} = \sqrt{(1+\gamma)^2U^2 - 1} = \sqrt{M^2-1}, \tag{71}$$

that is, it coincides with the Mach cone.

The profile of the light intensity across the oblique soliton can be obtained by a straightforward numerical integration of Eq. (68). In Fig. 8 we compare such a profile with the profile of the diffraction pattern obtained by direct numerical simulation using original Eqs. (5) and (6). Good agreement between these two profiles as well as characteristic behavior of the phase of the wave function shown in the lower panel of Fig. 8 confirm that the pattern in Fig. 2 inside the Mach cone

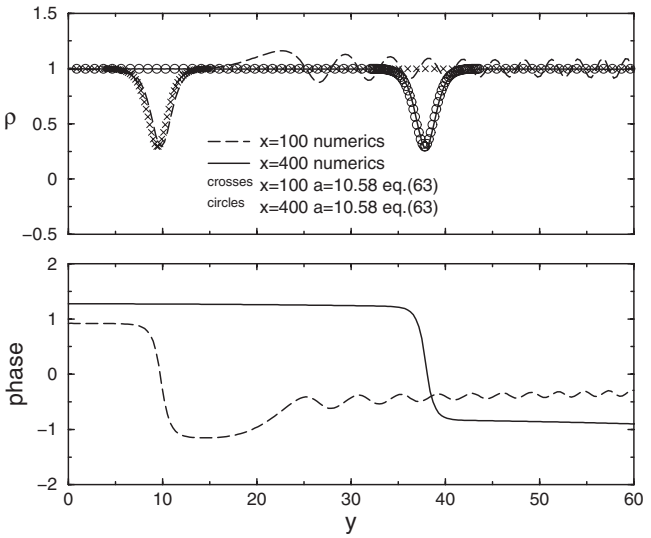

FIG. 8. Upper panel: Profiles of the intensity distributions for $x=100$ (dashed line), $x=400$ (solid line) and $y>0$ obtained from numerical solution of Eq. (5) with the nonlinear term given by Eq. (6) for $U=5$, $\gamma=0.2$, $z=120$. These profiles are compared with the soliton profiles obtained by solutions of Eq. (63) with slope $a=10.58$ shown as functions of y at the same values of x ($x=100$ corresponds to "crosses" and $x=400$ to "circles"). Lower panel: Profiles of the phase variation along the same cross sections of the numerically calculated wave function of the condensate. Jumps of phase correspond to the well-known behavior of the phase across dark solitons.

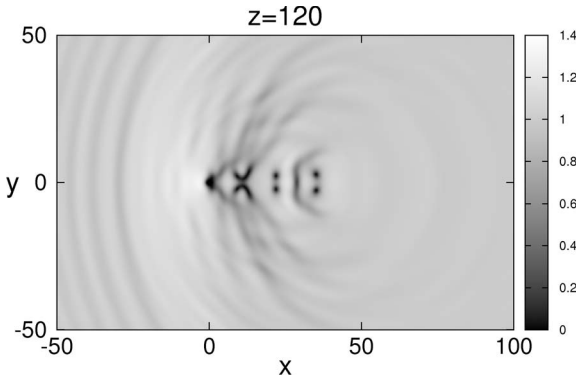

FIG. 9. Diffraction pattern at the output plane at the length $z=120$ and Mach number $M=0.9$. The patterns are obtained by numerical solution of Eq. (4) with $V(\mathbf{r})$ corresponding to an ideally reflecting wire with unit radius for $\gamma=0.2$.

indeed consists of oblique dark solitons generated by nonlinear diffraction of the light beam on the obstacle.

V. STABILITY OF OBLIQUE SOLITONS

The solitons profiles investigated in the preceding section are reached asymptotically as $z\to\infty$. However, the patterns calculated for finite z and shown in Fig. 2 indicate that some oscillations of intensity take place along the oblique solitons. Amplitude of these oscillations increases with distance from the obstacle which leads to generation of vortices at the end points of solitons. In fact, instability of dark 2D solitons with respect to transverse perturbations resulting in its nonlinear stage formation of vortices is well known (see [1]). Actually, just this instability prevents formation of dark solitons in the case of subsonic velocity of the flow. This situation is illustrated in Fig. 9 where the wave pattern at the output plane is shown for the Mach number $M=0.9$. As one can see, only vortices are generated because dark solitons are absolutely unstable and cannot be created as stationary structures of the diffraction pattern.

However, in the case of formation of dark solitons in the flow of Bose-Einstein condensate past an obstacle it was found [30] that the amplitude of oscillations decreases with growth of time at fixed distance from the obstacle for a large enough value of the oncoming flow velocity. This suggests that absolute instability of dark solitons transforms into their convective instability in the reference frame attached to the obstacle at some critical value of the flow velocity [31]. This means that wave packets built of unstable modes of the soliton's disturbance are convected so fast by the flow that instability cannot develop at a finite distance from the obstacle. The criterion of transition to the convective instability for a Bose-Einstein condensate evolving according to the Gross-Pitaevskii equation [see Eq. (7)] was derived in [31] and here we shall extend the analysis of [31] to the photorefractive Eq. (4).

A. Shallow solitons (Kadomtsev-Petviashvili approximation)

The theory is especially simple in the limit of small-amplitude solitons when the GNLS Eq. (5) can be reduced to the Kadomtsev-Petviashvili (KP) equation by means of standard reductive perturbation theory, which yields

$$\left(-2c_s\rho_z' + 2c_s^2\rho_{\tilde{x}}' + [3f'(\rho_0)+\rho_0 f''(\rho_0)]\rho'\rho_{\tilde{x}}' - \frac{1}{4}\rho_{\tilde{x}\tilde{x}\tilde{x}}'\right)_{\tilde{x}} + c_s^2\rho_{\tilde{y}\tilde{y}}' = 0, \tag{72}$$

where $\rho' \ll \rho_0$ denotes the intensity perturbation, small compared with the background intensity ρ_0, $\tilde{x}$ is a coordinate along a soliton, and $\tilde{y}$ is a transverse coordinate. We transform it to the standard form by introducing the new variables

$$\tilde{z} = \frac{z}{2c_s}, \quad \tilde{\xi} = \tilde{x} + c_s z, \quad \tilde{\eta} = \frac{\tilde{y}}{c_s},$$

$$\tilde{\rho} = -\frac{1}{3}[3f'(\rho_0)+\rho_0 f''(\rho_0)]\rho' \tag{73}$$

to obtain

$$\left(\tilde{\rho}_z + 3\tilde{\rho}\tilde{\rho}_{\tilde{\xi}} + \frac{1}{4}\tilde{\rho}_{\tilde{\xi}\tilde{\xi}\tilde{\xi}}\right)_{\tilde{\xi}} = \tilde{\rho}_{\tilde{\eta}\tilde{\eta}}. \tag{74}$$

As is well known, the KP equation (74) has the soliton solution

$$\tilde{\rho}_s = \frac{s}{\cosh^2[\sqrt{s}(\tilde{\xi}-s\tilde{z})]} = \frac{s}{\cosh^2(\sqrt{s}\{\tilde{x}+[c_s - s/(2c_s)]z\})}, \tag{75}$$

where the parameter s is small,

$$\frac{s}{c_s^2} \ll 1, \tag{76}$$

in accordance with the condition that the soliton is shallow. This solution is written in the reference frame with $\mathbf{u}\to\mathbf{0}$ as $x\to\infty$.

The soliton solution (75) is unstable with respect to transverse perturbations [38,39]. If we perturb the solution (75) along the $\tilde{y}$ axis,

$$\tilde{\rho} = \tilde{\rho}_s(\zeta) + \delta\tilde{\rho}, \quad \delta\tilde{\rho} = W(\zeta)\exp(\Gamma z + ip\tilde{y}), \quad \zeta = \tilde{x} + c\tilde{y}, \tag{77}$$

then in linear approximation we obtain equation for W:

$$[-W_{\zeta\zeta\zeta} + 4sW_\zeta - 12(\tilde{\rho}_s W)_\zeta]_\zeta - 4p^2 W = 4\Gamma W_\zeta. \tag{78}$$

This eigenvalue problem was studied in [39,40] where the following spectrum for the instability growth rate was obtained:

$$\Gamma(p) = (p/\sqrt{3})\sqrt{s - 2p/\sqrt{3}}. \tag{79}$$

Thus in the reference frame with $\mathbf{u}\to 0$ at $x\to\infty$ the soliton is absolutely unstable.

However, we are interested in the behavior of the soliton transformed to the reference frame "attached" to the obstacle by the substitution (64):

$$\tilde{\rho}_s = s\,\cosh^{-2}\left(\sqrt{\frac{s}{1+a^2}}\left\{x - ay + \left[\left(c_s - \frac{s}{2c_s}\right)\times\sqrt{1+a^2} - U\right]z\right\}\right). \tag{80}$$

The relationship between the soliton parameter s and the slope a follows from the condition that the oblique soliton solution does not depend on z:

$$s = c_s^2\left(1 - \frac{M^2}{1+a^2}\right), \tag{81}$$

where we took into account Eqs. (13) and (76). After the transformation to the "obstacle" frame we easily get the dispersion relation

$$\omega = \omega(p) = \mu p + i\frac{p}{\sqrt{3}}\sqrt{s - \frac{2p}{\sqrt{3}}},$$

$$\mu = U\,\sin\,\theta = \frac{Ma}{(1+\gamma)\sqrt{1+a^2}} \tag{82}$$

for waves propagating along the oblique soliton with the wave number p. The stability of the soliton is determined by the asymptotic behavior of the wave packets built of harmonic waves. Due to the term μp in the dispersion relation, the wave packets are convected by the flow along the soliton. If they are convected fast enough, then amplitude of the unstable disturbance cannot increase at a fixed distance from the obstacle and, as a result, the soliton is just convectively unstable [31]. As was shown in [31], for shallow KP solitons the criterion of transition from absolute to convective instability reads

$$\mu^2 > s. \tag{83}$$

Then substitution of Eqs. (81) for s and Eqs. (82) for μ gives at once

$$M > 1. \tag{84}$$

Thus the shallow solitons are convectively unstable for "supersonic" values of transverse wave vector U.

B. Deep solitons

Now we consider stability of soliton solutions of the photorefractive Eq. (4) with dropped external potential:

$$i\frac{\partial\psi}{\partial z} + \frac{1}{2}\Delta_\perp\psi - \frac{|\psi|^2}{1+\gamma|\psi|^2}\psi = 0. \tag{85}$$

Stability of solitons for the case of 2D NLS equation ($\gamma=0$) was studied in [41]. We shall write the soliton solution of Eq. (85) in the form

$$\psi_s(\zeta) = \sqrt{\rho_s(\zeta)}\,\exp\left(i\phi_s(\zeta) - \frac{iz}{1+\gamma}\right), \tag{86}$$

where $\rho_s(\zeta)$ is given by the solution of Eq. (68) and

$$\frac{\partial\phi_s}{\partial\zeta} = c\left(\frac{1}{\rho_s(\zeta)} - 1\right). \tag{87}$$

The disturbed function ψ can be taken in the form

$$\psi = \psi_s(\zeta) + (\psi' + i\psi'')\exp\left(i\phi_s(\zeta) - \frac{iz}{1+\gamma}\right). \tag{88}$$

Here ψ' and ψ'' depend on y and z as $\exp(ipy+\Gamma z)$. Substitution of Eq. (88) into Eq. (85) and linearization with respect to ψ' and ψ'' yields the linear spectral problem

$$\begin{pmatrix} -A & L_1 \\ L_2 & A \end{pmatrix}\begin{pmatrix} \psi'' \\ \psi' \end{pmatrix} = \Gamma\begin{pmatrix} \psi'' \\ -\psi' \end{pmatrix}, \tag{89}$$

where

$$A = \frac{c}{\rho_s}\left(\frac{\partial}{\partial\xi} - \frac{\rho_{s,\xi}}{2\rho_s}\right), \tag{90}$$

$$L_1 = \frac{1}{2}\frac{\partial^2}{\partial\xi^2} + \frac{1}{2}(c^2 - p^2) + \frac{1}{1+\gamma} - \frac{1}{2}\frac{c^2}{\rho_s^2} - \frac{3\rho_s + \gamma\rho_s^2}{(1+\gamma\rho_s)^2}, \tag{91}$$

$$L_2 = \frac{1}{2}\frac{\partial^2}{\partial\xi^2} + \frac{1}{2}(c^2 - p^2) + \frac{1}{1+\gamma} - \frac{1}{2}\frac{c^2}{\rho_s^2} - \frac{\rho_s}{1+\gamma\rho_s}. \tag{92}$$

The function ρ_s is considered here as known for a given value of the soliton velocity c; hence the system (89) can be solved numerically which yields the spectrum of the growth rate $\Gamma=\Gamma(p)$ for all values of c.

Again, we transform this solution to the reference frame attached to the obstacle and arrive at the dispersion relation

$$\omega(p) = \mu p + i\Gamma(p). \tag{93}$$

This equation determines implicitly the function $p=p(\omega)$. The type of stability is determined by the location of branching points p_{br} of this function (see, e.g., [42]) where $d\omega/dp=0$, which gives the equation

$$\mu = -i\frac{d\Gamma}{dp}, \tag{94}$$

which determines the branching point p_{br} as a function of μ at a given value of c. As was shown in [31], the critical value μ_{cr} for the transition from absolute to convective instability is determined by the condition that the function $p_{br}(\mu)$ has a branching point at $\mu=\mu_{cr}$. This gives the equation

$$\left.\frac{d^2\Gamma}{dp^2}\right|_{p=p_{cr}} = 0, \tag{95}$$

the solution of which gives the critical value p_{cr} for a given c. An example of the plot of the absolute value of the function $\Gamma(p)$ is shown in Fig. 10 for $\gamma=0.1$ and soliton velocity c corresponding to the minimal intensity $\rho_m=0.2$ and calculated by means of Eq. (69). It has an inflection point at $p=p_{cr}$ in the region where $\Gamma(p)$ is purely imaginary; thus p_{cr} can be calculated for a set of values of ρ_m in the interval $0 \le \rho_m \le 1$.

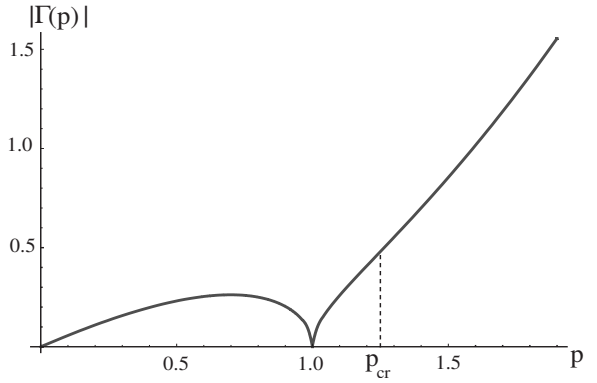

FIG. 10. Absolute value of the growth rate Γ as a function of the wave number p of a harmonic transverse perturbation for $\gamma=1$ and $\rho_m=0.2$.

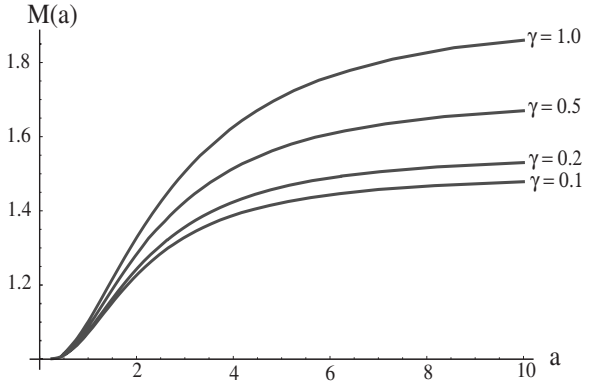

FIG. 11. Boundary between regions of absolute and convective instabilities for several values of the saturation parameter γ.

When p_{cr} is found as a function of ρ_m, we can substitute its value into Eq. (94) to obtain the critical value of μ, again, as a function of ρ_m:

$$\mu_{cr}(\rho_m) = -i \left. \frac{d\Gamma(p,\rho_m)}{dp} \right|_{p=p_{cr}}. \tag{96}$$

Now we substitute the relation

$$c = \frac{M}{(1+\gamma)\sqrt{1+a^2}} \tag{97}$$

into $\mu=Ma/[(1+\gamma)\sqrt{1+a^2}]$ to find $\mu=ca$ which gives the slope parameter as a function of ρ_m:

$$a(\rho_m) = \frac{\mu_{cr}(\rho_m)}{c(\rho_m)}, \tag{98}$$

where $c(\rho_m)$ is given by Eq. (69). At last, substitution of this function into Eq. (97) yields M_{cr} as a function of ρ_m:

$$M_{cr}(\rho_m) = (1+\gamma)c(\rho_m)\sqrt{1+a^2(\rho_m)}. \tag{99}$$

Equations (98) and (99) determine the critical value of the Mach number as a function of the slope a in a parametric form with $0 \le \rho_m \le 1$ playing a role of the parameter. Results of numerical computation of this function for several values of γ are shown in Fig. 11. Below these curves oblique solitons are absolutely unstable and cannot be created by the flow of light past an obstacle: perturbation of the flow behind the obstacle decays into vortices without formation of solitons. Above these curves, the oblique solitons become convectively unstable and their length grows faster than they decay into vortices. Hence vortices exist at the end points of solitons only and there is a region where the soliton profile is close to the stationary solution found in the preceding section, which was confirmed by numerical simulations.

VI. CONCLUSION

In this paper, we have developed the theory of formation of the wave pattern of light propagating through nonlinear photorefractive medium with a reflecting wire embedded in the medium. The light beam is supposed to be tilted with respect to the wire, which creates the "flow of light past an obstacle" analogous to that realized in experiments on superfluid flow of Bose-Einstein condensate past an obstacle. An analogy between propagation of light beams and superfluid dynamics suggests that a similar diffraction pattern can be observed in optical experiments. We have shown that the diffraction pattern consists of two regions separated by the "Mach cone." In the region outside the Mach cone the so-called "ship waves" are generated while inside this Mach cone the nonlinear dispersive shocks transforming into oblique soliton trains are situated. The simplest case, when just a single soliton is generated, is studied in detail. The main parameters of the oblique optical soliton are determined and it is shown that it is actually stable (more precisely, *convectively unstable*) with respect to small transverse perturbations for large enough values of transverse wave vector of the light beam. Detailed theory of ship waves is also given. All our findings are confirmed by numerical simulations. Since optical experiments seem more feasible than the experiments with ultracold gases, one may hope that our predictions could be verified experimentally.

ACKNOWLEDGMENTS

Work of E.G.K. and A.G. was supported by FAPESP/CNPq (Brazil) and work of Y.G.G. and A.M.K. was supported by RFBR (Russia).

[1] Yu. S. Kivshar and G. P. Agrawal, *Optical Solitons. From Fibers to Photonic Crystals* (Academic, Amsterdam, 2003).
[2] L. P. Pitaevskii and S. Stringari, *Bose-Einstein Condensation* (Cambridge University Press, Cambridge, England, 2003).
[3] T. B. Benjamin and M. J. Lighthill, Proc. R. Soc. London, Ser. A **224**, 448 (1954).
[4] R. Z. Sagdeev, in *Problems of Plasma Theory*, edited by M. A. Leontovich (Atomizdat, Moscow, 1964), Vol. 5 (in Russian).
[5] G. B. Whitham, Proc. R. Soc. London, Ser. A **283**, 238 (1965).
[6] A. V. Gurevich and L. P. Pitaevskii, Zh. Eksp. Teor. Fiz. **65**, 590 (1973) [Sov. Phys. JETP **38**, 291 (1974)].
[7] H. Flaschka, M. G. Forest, and D. W. McLaughlin, Commun. Pure Appl. Math. **33**, 739 (1980).
[8] B. A. Dubrovin and S. P. Novikov, Russ. Math. Surveys **44**, 35 (1989).
[9] S. P. Tsarev, Izv. Akad. Nauk SSR Ser. Fiz. Mat. Nauk **54**, 1048 (1990) [Math. USSR, Izv. **37**, 397 (1991)].
[10] A. V. Gurevich, A. L. Krylov, and G. A. El, Zh. Eksp. Teor. Fiz. **101**, 1797 (1992) [Sov. Phys. JETP **74**, 957 (1992)].
[11] A. M. Kamchatnov, *Nonlinear Periodic Waves and Their Modulations—An Introductory Course* (World Scientific, Singapore, 2000).
[12] G. A. El, Chaos **15**, 037103 (2005).
[13] M. H. Anderson, J. R. Ensher, M. R. Matthews, C. E. Wieman, and E. A. Cornell, Science **269**, 198 (1995).
[14] K. B. Davis, M.-O. Mewes, M. R. Andrews, N. J. van Druten, D. S. Durfee, D. M. Kurn, and W. Ketterle, Phys. Rev. Lett. **75**, 3969 (1995).
[15] C. C. Bradley, C. A. Sackett, J. J. Tollett, and R. G. Hulet, Phys. Rev. Lett. **75**, 1687 (1995); C. C. Bradley, C. A. Sackett, and R. G. Hulet, *ibid.* **78**, 985 (1997).
[16] B. Damski, Phys. Rev. A **69**, 043610 (2004).
[17] A. M. Kamchatnov, A. Gammal, and R. A. Kraenkel, Phys. Rev. A **69**, 063605 (2004).
[18] T. P. Simula, P. Engels, I. Coddington, V. Schweikhard, E. A. Cornell, and R. J. Ballagh, Phys. Rev. Lett. **94**, 080404 (2005).
[19] M. A. Hoefer, M. J. Ablowitz, I. Coddington, E. A. Cornell, P. Engels, and V. Schweikhard, Phys. Rev. A **74**, 023623 (2006).
[20] P. Engels and C. Atherton, Phys. Rev. Lett. **99**, 160405 (2007).
[21] W. Wan, S. Jia, and J. W. Fleischer, Nat. Phys. **3**, 46 (2007).
[22] N. Ghofraniha, C. Conti, G. Ruocco, and S. Trillo, Phys. Rev. Lett. **99**, 043903 (2007).
[23] C. Barsi, W. Wan, C. Sun, and J. W. Fleischer, Opt. Lett. **32**, 2930 (2007).
[24] S. Jia, W. Wan, and J. W. Fleischer, Phys. Rev. Lett. **99**, 223901 (2007).
[25] G. A. El, A. Gammal, E. G. Khamis, R. A. Kraenkel, and A. M. Kamchatnov, Phys. Rev. A **76**, 053813 (2007).
[26] L. D. Landau and E. M. Lifshitz, *Fluid Mechanics* (Pergamon, Oxford, 1987).
[27] V. I. Karpman, *Nonlinear Waves in Dispersive Media* (Nauka, Moscow, 1973).
[28] A. V. Gurevich, A. L. Krylov, V. V. Khodorovskii, and G. A. El, JETP **81**, 87 (1995); **82**, 709 (1996).
[29] G. A. El and A. M. Kamchatnov, Phys. Lett. A **350**, 192 (2006); **352**, 554(E) (2006).
[30] G. A. El, A. Gammal, and A. M. Kamchatnov, Phys. Rev. Lett. **97**, 180405 (2006).
[31] A. M. Kamchatnov and L. P. Pitaevskii, Phys. Rev. Lett. **100**, 160402 (2008).
[32] G. B. Whitham, *Linear and Nonlinear Waves* (Wiley-Interscience, New York, 1974).
[33] I. Carusotto, S. X. Hu, L. A. Collins, and A. Smerzi, Phys. Rev. Lett. **97**, 260403 (2006).
[34] Yu. G. Gladush, G. A. El, A. Gammal, and A. M. Kamchatnov, Phys. Rev. A **75**, 033619 (2007).
[35] Yu. G. Gladush and A. M. Kamchatnov, Zh. Eksp. Teor. Fiz. **132**, 589 (2007) [JETP **105**, 520 (2007)].
[36] G. A. Swartzlander, Jr. and C. T. Law, Phys. Rev. Lett. **69**, 2503 (1992).
[37] G. E. Astrakharchik and L. P. Pitaevskii, Phys. Rev. A **70**, 013608 (2004).
[38] B. B. Kadomtsev and V. I. Petviashvili, Sov. Phys. Dokl. **15**, 539 (1970) [Dokl. Akad. Nauk SSSR **192**, 753 (1970)].
[39] V. E. Zakharov, JETP Lett. **22**, 172 (1975) [Zh. Eksp. Teor. Fiz. Pis'ma Red. **22**, 304 (1975)].
[40] J. C. Alexander, R. L. Pego, and R. L. Sachs, Phys. Lett. A **226**, 187 (1997).
[41] E. A. Kuznetsov and S. K. Turitsyn, Sov. Phys. JETP **67**, 1583 (1988) [Zh. Eksp. Teor. Fiz. **94**, 119 (1988)].
[42] E. M. Lifshitz and L. P. Pitaevskii, *Physical Kinetics* (Pergamon, London, 1981).